Growing and Testing a Zinc-Oxide Piezoelectric Sensor for Pressure Sensing Applications

Carter Chapman, Flor Nardone, Saki Male, and Ingrid Russell
UNC Chapel Hill Department of Physics

(Physics 481L, Group E)

(Dated: May 2026)

Zinc oxide (ZnO) thin films were fabricated and characterized for use as piezoelectric pressure sensors. Films were deposited on fluorine-doped tin oxide (FTO) substrates by pulsed laser deposition (PLD) at 20 Hz and 178 mJ laser energy in a 5 mTorr oxygen atmosphere, and silver top electrodes were subsequently deposited to form vertical-stack FTO/ZnO/Ag devices. Post-deposition thermal annealing at 500°C was used to improve crystallographic orientation and film quality. X-ray diffraction confirmed strong c-axis preferred orientation in the best-annealed sample (Sample 21), with substantially narrower Zinc Oxide (ZnO) peak widths and fewer non-(00l) reflections than observed in unannealed control films. Device electrical response was measured using a custom high-impedance instrumentation amplifier rig (AD620-based, Arduino-logged, calibrated gain $G = 62.5$). DC resistance measurements across the sample set revealed parasitic shunt conduction spanning more than three orders of magnitude, with Sample 21 exhibiting the highest measured value of approximately 107 kΩ. Single-event mechanical stimulation produced no detectable voltage response above the ambient noise floor, but rhythmic cyclical tapping on Sample 21 produced a clearly correlated voltage pattern. This signal satisfied three independent artifact-rejection control (persistence under an insulating tape layer, clean polarity inversion on electrode reversal, and absence when the bare substrate was stimulated instead of the active Ag pad) collectively providing evidence of piezoelectric origin. Future work will require more sensitive measurement equipment to more precisely quantify the piezoelectric response of these ZnO thin film sensors.

I. INTRODUCTION

Zinc oxide is a promising material for piezoelectric pressure sensing because it combines a non-centrosymmetric wurtzite crystal structure with relatively simple and low-cost thin-film fabrication.[1, 2] In a piezoelectric material, applied mechanical stress produces an electrical polarization, allowing pressure or force to be converted directly into a measurable electrical signal. This makes ZnO attractive for sensor applications, particularly in cases where a thin-film device geometry is desired.[1] In addition to its piezoelectric behavior, ZnO has a room-temperature band gap of approximately 3.3 eV and can be grown as a thin film using pulsed laser deposition (PLD), making it well-suited for laboratory-scale device fabrication and characterization.[1, 2]

For ZnO thin films to function effectively as piezoelectric pressure sensors, the crystallographic structure of the film is especially important.[2]The strongest piezoelectric response is expected when the film exhibits growth along the c-axis of the wurtzite lattice, since this is the direction along which the greatest charge displacement occurs under applied stress.[1] In the device architecture used in this work, ZnO was deposited on fluorine-doped tin oxide (FTO), which served as the bottom electrode, and silver (Ag) was deposited on top of the ZnO to form the upper electrode and complete the sensor structure. Because device performance depends not only on the presence of ZnO, but also on film thickness, crystallinity, and electrical isolation between the electrodes, the project required both fabrication optimization and structural characterization before meaningful sensor testing could be carried out.

The central goal of this project was to grow ZnO thin films suitable for piezoelectric sensing and to fabricate a device capable of producing a measurable electrical response under applied pressure. To do this, PLD growth conditions were refined through multiple deposition trials in which substrate type, oxygen pressure, pulse count, and preparation methods were adjusted in order to produce films of appropriate thickness and quality. After establishing workable deposition conditions, Ag electrodes were added, and the resulting devices were examined using X-ray diffraction (XRD) and electrical testing. Annealing was also introduced as a way to improve film crystallinity and encourage more consistent ZnO orientation. These steps were necessary because the usefulness of the final device depends on both the structural quality of the ZnO film and the ability to preserve the small electrically generated signal at the measurement stage.

A major experimental challenge in this work is that the expected piezoelectric signal from a ZnO thin film of this geometry is very small. As estimated in the current paper, the voltage response under the pressures achievable in the lab is expected to be on the order of microvolts, which places the signal close to or below the noise floor of standard measurement equipment. Earlier testing with a multimeter and probe station showed that conventional approaches were not well matched to the open-circuit, transient nature of the signal being sought, motivating the use of a more specialized amplification and measurement strategy. As a result, this project became not only a study of thin-film growth and structural characterization, but also an investigation into the practical limitations involved in measuring the electromechanical response of ZnO thin-film devices in a laboratory setting.

In this work, ZnO thin films were grown on FTO substrates by PLD, integrated with Ag electrodes, and evaluated as candidate piezoelectric pressure sensors. XRD was used to assess film structure and orientation, including the effect of annealing on crystallinity, while electrical measurements were used to test whether the fabricated devices could produce a detectable pressure-induced signal. Although the fabrication and structural characterization of the films were successful, the results also show that measurement sensitivity and parasitic conduction paths place important limits on device performance. Taken together, this work demonstrates both the promise of ZnO as a thin-film piezoelectric sensing material and the experimental challenges that must be overcome to realize a reliable pressure sensor in this geometry.

II. THEORETICAL BACKGROUND

A. Crystal Structure

ZnO is a wurtzite structured semi-conductor that exhibits piezoelectric behavior due to its non-centrosymmetric crystal structure.[1] When ZnO is in its equillbrium state, each Zinc (Zn^{2+}) ion is tetrahedrally coordinated by four oxygen (O^{2-}) ions, and vice versa.

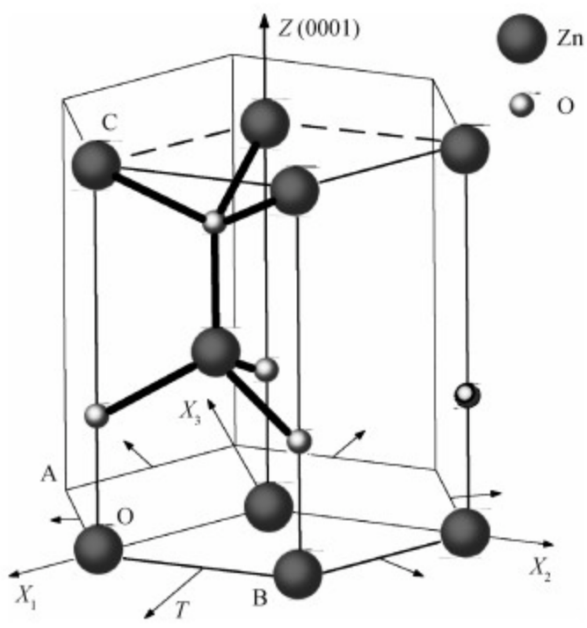

FIG. 1: Crystal structure of ZnO.

Under zero applied stress, the charges within each unit cell coincide, and there is no dipole moment in the lattice. However, when external mechanical stress (σ) is applied, the atoms shift. The Zn^{2+}, and O^{2-} atoms are shifted unequal distances from each other, creating a dipole moment in the crystal.[1] The strongest dipole moment arises from applying stress normal to the c-axis of the crystal shown in Figure 1.[1]It is represented by Miller indices also shown on the figure, notated by (x,y,z). When this dipole moment is created, a potential difference can be measured and applied as a signal for a pressure sensor.

The piezoelectric response of the ZnO is largely dependent on the quality of the crystal and whether the ZnO is grown in a crystalline.[2]

B. Effect of Stress on Film Resistivity

While the direct piezoelectric effect describes the generation of a macroscopic voltage in response to applied stress, ZnO is simultaneously a semiconductor, meaning that mechanical stress also influences the electrical resistivity of the film through several coupled mechanisms.[1] Understanding these effects is important for interpreting sensor behavior, particularly any deviations from the idealized linear voltage response.

The resistivity of a semiconductor film is given by:

$$\rho = \frac{1}{n \cdot e \cdot \mu} \tag{1}$$

where n is the free carrier concentration (m^{-3}), e is the elementary charge, and μ is the carrier mobility ($m^2\ V^{-1}\ s^{-1}$). Applied mechanical stress can alter both n and μ simultaneously, making the resistivity of ZnO stress-dependent.

C. Predicted Electrical Response

The relationship between applied mechanical stress and the resulting electric polarization is governed by:

$$P_i = d_{ijk} \cdot \sigma_{jk} \tag{2}$$

where P_i is the electric polarization (C/m^2), σ_{jk} is the mechanical stress tensor (Pa), and d_{ijk} is the third-rank piezoelectric coefficient tensor (C/N). For a ZnO thin film oriented along its c-axis, where the applied force is perpendicular to the film surface, this simplifies to the one-dimensional form:

$$P = d_{33} \cdot \sigma \tag{3}$$

where d_{33} is the piezoelectric coefficient along the polar axis of the crystal.

D. Piezoelectric coefficient

The piezoelectric response of a material is characterized by several coefficients. The two most relevant for this work are:

- **Piezoelectric charge coefficient (d_{33}):** Describes the amount of electric charge generated per unit of applied force, or equivalently, the mechanical strain produced per unit electric field. For ZnO, the bulk value is approximately $d_{33} \approx 12.4$ pC/N, though thin film values can range from 2–12 pC/N depending on deposition method and film quality [3].

- **Piezoelectric voltage coefficient (g_{33}):** Describes the electric field generated per unit of applied mechanical stress. It is related to d_{33} by:

$$g_{33} = \frac{d_{33}}{\varepsilon_{33}} \tag{4}$$

where ε_{33} is the dielectric permittivity of ZnO along the polar axis, given by:

$$\varepsilon_{33} = \varepsilon_r \cdot \varepsilon_0 \tag{5}$$

with $\varepsilon_r = 8.66$ (relative permittivity of ZnO) and $\varepsilon_0 = 8.85 \times 10^{-12}$ F/m (permittivity of free space).

E. Voltage Response to Applied Pressure

Under open-circuit conditions, where no current flows through the device, the voltage generated across a ZnO film of thickness t under an applied pressure σ is:

$$V = g_{33} \cdot \sigma \cdot t \tag{6}$$

Substituting the expression for g_{33}:

$$V = \frac{d_{33}}{\varepsilon_{33}} \cdot \sigma \cdot t \tag{7}$$

This can also be expressed in terms of applied force F over electrode area A, since $\sigma = F/A$:

$$V = \frac{d_{33} \cdot F \cdot t}{\varepsilon_{33} \cdot A} \tag{8}$$

F. Expected Linear Behavior

From Equation (5), the predicted voltage output is directly proportional to the applied pressure σ. Since g_{33}, ε_{33}, d_{33}, and t are all material and geometric constants for a given film, the voltage response takes the form:

$$V = k \cdot \sigma \tag{9}$$

where $k = g_{33} \cdot t$ is a constant sensitivity factor (V/Pa). This indicates that the sensor is expected to follow a **linear relationship** between applied pressure and output voltage. The slope of this linear response is directly controlled by:

- The piezoelectric coefficient d_{33}, which is an intrinsic material property dependent on film quality and crystallographic orientation

- The film thickness t, where a thicker film produces a proportionally higher voltage for the same applied pressure

- The dielectric permittivity ε_{33}, which is a fixed material property for ZnO

Any deviation from this linear behavior in experimental measurements may indicate non-ideal effects such as charge leakage, film inhomogeneity, substrate clamping effects, or nonlinear elastic behavior at higher pressures.

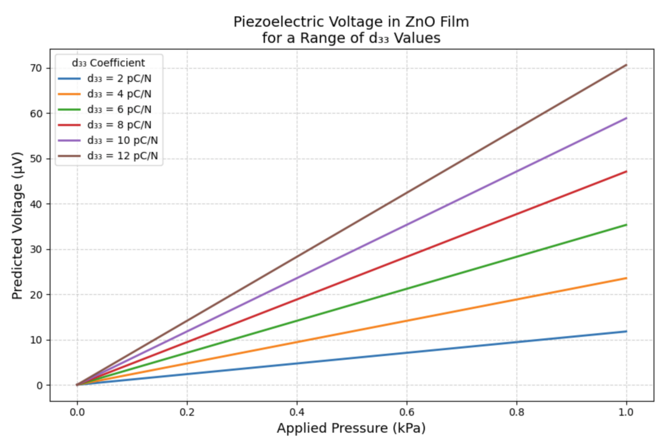

FIG. 2: Plot comparing the applied pressure and potential difference from the separation of charges along the c-axis of the ZnO thin film. The relationship is shown for different values of d_{33}.

Figure 2 allows us to estimate what the expected potential difference should be depending on the amount of pressure we apply to the thin film. Generally with the tools in the lab we expect this potential difference to be on the order of μV, meaning low noise is required for this measurement.

III. METHODS

A. Device Creation

Our thin film devices were fabricated using a pulsed laser deposition (PLD) system. The laser was operated at 20 Hz and an energy of 178 mJ with power fluctuating between 0.65 and 0.76 W. Prior to the deposition, both Ag and Zn targets were cleaned with 2000 pulses. ZnO layers were deposited in 5 mtorr O2 at a setpoint flow rate of 10 sccm by running 20000 pulses with the substrate on the low setting. Afterwards, the film was masked using a custom holder to define two smaller rectangular regions, where Ag was deposited under vacuum for 10000 pulses.

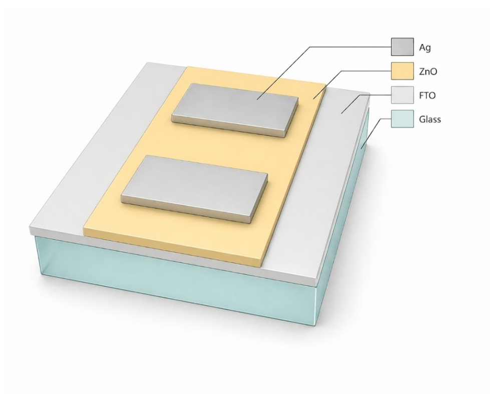

FIG. 3: Diagram of our device set up.

The crystallographic structures of the ZnO thin films and FTO substrate were analyzed using X-ray diffraction (XRD). Measurements were performed with a Rigaku SmartLab theta-theta diffractometer, allowing the Miller indices of each thin film to be determined and their preferred orientation to be identified.

To improve consistency and intensity of ZnO thin film orientation, an annealing process was developed. Samples were annealed in a timed oven: they were ramped up to 500 degrees C over the course of one hour, held at that temperature for one hour, and then ramped down to room temperature over the course of one hour.

B. Electrical Characterization

1. *Rationale for Measurement Topology*

Thin-film piezoelectric devices present two fundamental challenges to electrical characterization. First, although the material-level response of a piezoelectric crystal is a static polarization proportional to applied stress, the electrical signal accessible at the device terminals is effectively transient under any measurement employing a finite-impedance voltage amplifier: the device is correctly modeled as a current source $i(t) = d_{33}\, dF/dt$ in parallel with the film capacitance, and any stored charge leaks through the finite parallel resistance of the device itself, of the measurement input, and of the surrounding environment (humidity-mediated surface conduction) on a timescale $\tau = RC$. In the low-R regime characteristic of our devices, this timescale is of microsecond order, and the measurement responds effectively to dF/dt rather than to F. Standard DC voltmeters and source-measure units, which are optimized for static voltage or current measurement, are poorly matched to this behavior; the measurement system must instead be fast enough to capture the brief transients generated during force changes. Second, the expected signal amplitude is small—of order 10–100 μV for thin films of the geometry used in this work—while the device impedance is high (typically megohms or greater in a working device), which together make the measurement extremely susceptible to electromagnetic pickup, triboelectric contamination, and loading by the measurement instrument itself.

To address these constraints, a differential high-input-impedance instrumentation amplifier was chosen as the measurement front-end. Instrumentation amplifiers provide three properties that match the requirements of a piezoelectric measurement: high differential input impedance (typically 10^{10} Ω in the case of the AD620), which minimizes loading of the high-impedance device; high common-mode rejection ratio (nominally 100 dB), which suppresses the electromagnetic interference that inevitably couples equally onto both leads of a differentially wired sensor; and user-adjustable gain, which can be tuned to place the device signal within the dynamic range of a downstream analog-to-digital converter.

2. *Circuit Wiring and Grounding*

Module power was supplied from the 5 V rail of an Arduino Uno microcontroller board, with the negative-rail output pin (V–) of the module left deliberately disconnected to avoid damage to the onboard charge pump. The amplifier's differential signal inputs, S+ and S–, were connected via jumper wires respectively to the Ag top electrode and to the exposed FTO bottom electrode of the device under test. Module ground and Arduino ground shared a common reference node on the breadboard. The amplifier output Vout was connected directly to the Arduino analog input pin A0. Because the module was powered from the Arduino's 5 V rail and its output buffer saturates at approximately $V_{\text{in}} - 2$ V ≈ 3 V, the amplifier output is physically limited to a voltage well within the 0–5 V safe operating range of the Arduino analog input, and no series current-limiting resistor or voltage divider was required between Vout and A0.

3. *Gain and Offset Calibration*

Before each measurement session, amplifier gain was calibrated using a precision resistive divider that in-jected a known differential test voltage at the amplifier inputs. The divider comprised two 30 kΩ resistors and one 270 Ω resistor in series across the 5 V Arduino supply, producing a differential test signal of $V_{\text{test}} = 5\text{ V} \times 270/(30{,}000 + 30{,}000 + 270) = 22.4$ mV at the junction between the 270 Ω resistor and ground. This test voltage was applied to S+ with S– tied to the breadboard ground, and the resulting amplifier output V_{out} was measured with a DMM. Amplifier gain was calculated as $G = (V_{\text{out}} - V_{\text{baseline}})/V_{\text{test}}$, where V_{baseline} was the output voltage measured with S+ and S– both tied to ground (zero differential input). After adjustment, the gain was measured to be $G = 62.5$ and the baseline was set to $V_{\text{baseline}} = 1.5$ V, placing the resting output near the midpoint of the amplifier's 0–3 V swing range so that both positive and negative piezoelectric pulses could be accommodated without clipping.

Before each measurement, the baseline was verified, and the offset trimpot W103 was adjusted if necessary to return the resting output to 1.5 V with inputs shorted. This re-check ensured that thermal drift between sessions would not exhaust the available headroom.

4. Gain and Offset Calibration

Before each measurement session, amplifier gain was calibrated using a precision resistive divider that in-
jected a known differential test voltage at the amplifier inputs. The divider comprised two 30 kΩ resistors and one 270 Ω resistor in series across the 5 V Arduino supply, producing a differential test signal of $V_{\text{test}} = 5\text{ V} \times 270/(30{,}000 + 30{,}000 + 270) = 22.4$ mV at the junction between the 270 Ω resistor and ground. This test voltage was applied to S+ with S– tied to the breadboard ground, and the resulting amplifier output V_{out} was measured with a DMM. Amplifier gain was calculated as $G = (V_{\text{out}} - V_{\text{baseline}})/V_{\text{test}}$, where V_{baseline} was the output voltage measured with S+ and S– both tied to ground (zero differential input). After adjustment, the gain was measured to be $G = 62.5$ and the baseline was set to $V_{\text{baseline}} = 1.5$ V, placing the resting output near the midpoint of the amplifier's 0–3 V swing range so that both positive and negative piezoelectric pulses could be accommodated without clipping.

Before each measurement, the baseline was verified, and the offset trimpot W103 was adjusted if necessary to return the resting output to 1.5 V with inputs shorted. This re-check ensured that thermal drift between sessions would not exhaust the available headroom.

5. Data Acquisition

The amplifier output was digitized by the Arduino's onboard 10-bit successive-approximation ADC, which divides the 0–5 V input range into 1024 discrete levels (4.88 mV per level). The ADC prescaler was modified from its default value of 128 to 16, increasing the effective conversion rate from approximately 9.6 kHz to approximately 77 kHz and allowing a sustained measurement sample rate of 2 kHz without introducing sample-to-sample timing jitter. This sample rate meets the Nyquist criterion for the millisecond-scale piezoelectric pulses expected from manual mechanical stimulation (whose principal frequency content lies below approximately 1 kHz) and provides sufficient temporal resolution to distinguish discrete tap-and-release events.

Firmware running on the Arduino implemented two signal-processing steps. First, at start-up, a two-second window of ADC samples was averaged to determine the resting baseline voltage V_{baseline} at the amplifier output; during this window, the device was left undisturbed so that the captured baseline reflected only DC offset and not any transient response. Second, during measurement, each digitized sample V_{out} was converted to a sensor-referred voltage via

$$V_{\text{sensor}} = (V_{\text{out}} - V_{\text{baseline}})/G. \tag{10}$$

A slowly tracking exponential moving average with a time constant of approximately one second served as an adaptive baseline, providing a software high-pass filter that rejects DC drift (thermal, contact-potential) while passing the fast piezoelectric transients of interest. To enable comparison between measurements, the Arduino firmware transmitted two fixed-amplitude anchor values alongside each data sample, which were used to pin the vertical scale of the Arduino IDE's Serial Plotter display at a fixed range.

6. Noise Floor and System Verification

Before each measurement, a 30-second record of the amplified output was acquired with the sensor connected but undisturbed. The peak-to-peak excursion of this record characterized the system noise floor in the specific electromagnetic environment of the lab bench. Across the measurements reported in this work, the typical noise floor ranged from 200 to 500 μV referred to the sensor input, with the dominant contribution identified as 60 Hz mains pickup rather than thermal (Johnson) noise. Placement of the probe leads in close parallel, shortening of unshielded wire runs, and separation of the measurement bench from laptop power supplies and fluorescent lighting were all observed to reduce the pickup amplitude, consistent with electromagnetic origin.

Two further tests verified that the measurement chain was functioning end-to-end. First, with S+ left floating (not connected to any source) and S– grounded, touching the bare end of the S+ input lead with a fingertip produced a large 60 Hz signal on the plot, confirming that the amplifier was correctly amplifying its differential input. Second, on connection of the device to the amplifier, the free-lead 60 Hz signal disappeared, consistent with the device's finite differential resistance providing a low-impedance termination between S+ and S– that, combined with the AD620's high common-mode rejection ratio, strongly suppresses symmetric pickup.

7. Mechanical Stimulation and Control Protocol

Mechanical stimulation was applied to the Ag top electrode using a rigid, electrically insulating plastic probe tip held and brought into controlled contact with the pad; the probe tip served as the mechanical coupling element between the experimenter's hand and the device. The insulating tip was chosen deliberately to avoid establishing any conductive path between the experimenter's body and the measurement circuit. Using a nonconductive plastic tip isolates the force input from any such electrical pathway, so that the observed signal reflects only the device's response to mechanical stimulus. Three distinct modes of stimulation were applied: (i) a firm single-contact tap as a discrete event; (ii) sustained press-and-hold loading with approximately constant applied force; and (iii) rhythmic cyclical tapping at approximately 2 Hz, sustained over several seconds.

To distinguish genuine piezoelectric response from common artifacts, three independent control experiments were performed following any candidate positive signal observation:

1. **Tape-insulation control:** a layer of adhesive tape was placed between the stimulating plastic probe tip (as well as between a metal conductive nut we previously attempted to use) and the Ag pad, eliminating direct plastic-to-metal (and previously metal-to-metal) contact at the active surface. A persistent signal through the tape rules out triboelectric contact-electrification as the signal origin, because triboelectric charging requires direct contact between dissimilar materials and is eliminated by an intervening insulator layer.

2. **Electrode-polarity reversal control:** the S+ and S– probe connections were exchanged, so that the Ag top electrode was now connected to the inverting input and the FTO bottom electrode to the non-inverting input. A genuine piezoelectric signal must invert cleanly in sign under this operation without change in amplitude, because the polarity of the piezoelectric surface charge is tied to the fixed polar axis of the crystal and is independent of the external measurement reference frame. Artifacts arising from electromagnetic pickup, thermal drift, or mechanical microphonics do not, in general, invert cleanly under electrode swap.

3. **Off-device mechanical control:** mechanical stimulation was applied to the bare glass substrate at a location distant from any Ag pad, while the measurement probes remained attached to an active Ag pad. The absence of any correlated signal in this configuration rules out signal generation via mechanical vibration coupled through the substrate, sample holder, or probe station—since any vibration so coupled would produce the same signal regardless of where force was applied.

IV. RESULTS

A. ZnO Crystal Growth

We took XRD measurements of 7 samples. One glass substrate, one FTO-layered glass, one nonannealed ZnO, and two annealed ZnO samples.

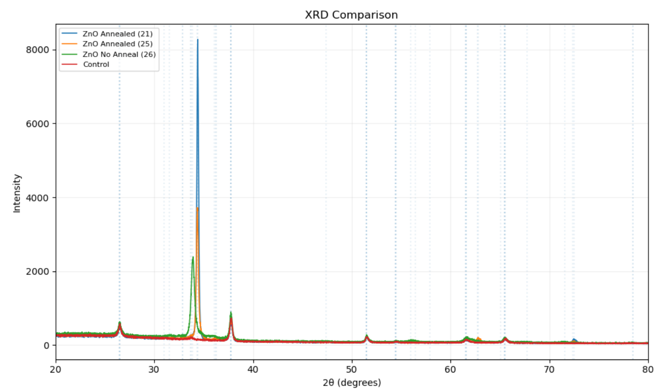

FIG. 4: The intensity of 2 theta peaks from XRD measured thin ZnO thin films and a control.

The XRD scan of Sample 21 (Fig. 4) is strongly dominated by the ZnO wurtzite (002) reflection at $2\theta = 34.39°$ ($d = 2.606$ Å), with a peak intensity of approximately 2.4×10^5 cps and a full width at half maximum of 0.18°. This (002) peak is approximately 39 times larger in intensity than the next-strongest ZnO reflection—the (101) peak at $2\theta = 36.25°$—and also much larger than the weaker (103), (112), and (004) ZnO reflections observed at higher 2θ. The dominance of the (002) reflection over all other observed ZnO orientations indicates a strong c-axis preferred orientation normal to the substrate. A second-order ZnO (004) reflection at $2\theta = 72.49°$ is also visible at lower intensity ($\sim 5.5 \times 10^3$ cps), further confirming c-axis stacking. Analysis of the (002) peak width yields a ZnO crystallite size of approximately 49 nm along the c-axis. This strong c-axis growth is observed in other annealed samples (like sample 25), but not as strongly as in sample 21. We continued our testing on sample 21, as it would produce more favorable results.

The remaining peaks in the Sample 21 scan—at $2\theta =$ 26.46°, 37.74°, 51.50°, 61.60°, and 65.50°—are indexed to the (110), (200), (211), (310), and (301) reflections of SnO_2 (cassiterite) and originate from the FTO bottom electrode rather than from the ZnO film. These same reflections appear in the reference scan of the bare FTO-coated glass substrate at comparable intensities, confirming that they are not piezoelectrically active features.

ZnO (*hkl*)	Sample 21 (annealed) 2θ (°)	Intensity (cps)	FWHM (°)	Sample 26 (unannealed) 2θ (°)	Intensity (cps)	FWHM (°)
(100)	—	—	—	31.52	8,760	1.79
(002)	34.39	243,020	0.18	33.89*	64,850*	0.38*
(101)	36.25	6,200	0.31	36.10	7,240	2.36
(110)	—	—	—	54.45	3,810	0.24
(103)	62.77	4,600	0.47	61.56*	6,140*	0.93*
(112)	67.77	3,130	0.13	65.45*	6,680*	0.34*
(004)	72.49	5,530	0.26	71.53	2,950	0.84

TABLE I: Observed ZnO diffraction peaks in Sample 21 (annealed) and Sample 26 (unannealed), extracted from the Rigaku SmartLab θ–2θ scans. Dashes (—) indicate reflections not observed in the scan. Asterisks (*) mark peaks that overlap with SnO_2 substrate reflections and therefore include both ZnO and SnO_2 contributions in their reported intensity and width.

The XRD scan of the unannealed ZnO control film (Sample 26) differs qualitatively from Sample 21 (Table I) and establishes the role of annealing in developing c-axis texture. Sample 26 exhibits multiple non-(00l) ZnO reflections at substantial intensities—(100) at $2\theta = 31.52°$, (101) at $2\theta = 36.10°$, and (110) at $2\theta = 54.45°$—all absent from Sample 21; the ZnO (100) reflection in particular is a direct fingerprint of a-axis or randomly oriented grains. The ZnO (101) reflection common to both scans is approximately eight times broader in Sample 26 (FWHM 2.36°) than in Sample 21 (FWHM 0.31°), and the (004) reflection shows the same trend (0.84° versus 0.26°); broader peaks correspond to smaller and less ordered crystallites, consistent with thermally-driven grain growth during the anneal. The apparent (002) feature in Sample 26 at $2\theta = 33.89°$ overlaps the SnO_2 (101) substrate reflection and cannot be cleanly attributed to c-axis ZnO alone.

The contrast between the two scans is unambiguous: the as-deposited film is polycrystalline with mixed orientation and small grain size, while the annealed Sample 21 (and 25) is strongly c-axis textured with much larger grains. The post-deposition anneal is directly responsible for both the development of c-axis preferred orientation and the coarsening of the crystallite microstructure. The second annealed ZnO sample (not shown in detail) exhibits an intermediate pattern—a (002) reflection present but weaker than Sample 21, and with weaker residual non-(00l) reflections—confirming that Sample 21 is the most fully c-axis-oriented device produced in this work.

A qualitative visual change also accompanied the annealing step: the as-deposited ZnO films appeared light brown to yellow in color, and became notably more transparent and visually clear after the anneal. Stoichiometric ZnO has a direct bandgap of approximately 3.3 eV, which places its absorption edge in the near-ultraviolet and makes the material nominally transparent across the visible spectrum. Oxygen-deficient ZnO films grown in low-O_2-pressure PLD contain a substantial population of native point defects—principally oxygen vacancies—that introduce defect levels within this bandgap. These mid-gap defect states absorb sub-bandgap visible light and account for the yellow-brown tint of as-deposited films. Annealing in air drives oxygen diffusion into the film, reduces the density of these defect states, and eliminates the sub-bandgap absorption, restoring visible transparency. The observed transparency improvement is consistent with the reduction of native-defect density invoked in Section IV.B to explain the annealing-induced increase in bulk resistivity.

B. DC Electrical Characterization/Response

Two-probe DC resistance measurements were performed on every Ag/FTO electrode pair of each fabricated device using a handheld digital multimeter. The DMM was applied in a brief touch-and-release manner in order to minimize the time that the test current was applied to the device. Across the fabricated sample set, measured DC resistance values spanned more than three orders of magnitude. At the low end of the distribution, several electrode pairs (including, for example, Sample 20) registered as fully shorted, with measured resistance below the lower detection limit of the meter and no distinguishable voltage drop at the DMM's test current. These devices exhibited direct metallic continuity between the Ag top electrode and the FTO bottom electrode and behaved electrically as closed switches. Other devices produced finite but still low resistance values, ranging from approximately 800 Ω on Sample 23 up to a maximum of approximately 107 kΩ on Sample 21. Representative intermediate values included approximately 12.5 kΩ on Sample 27 and approximately 78 kΩ on Sample 24. Note that out of the samples that we found not to be shortened, annealed samples seemed to correlate with higher resistance value measurements.

A well-behaved piezoelectric capacitor of this geometry would be expected to exhibit a DC resistance of order megaohms or greater, consistent with the high-resistivity insulating ZnO required for piezoelectric sensing [?]. All measured devices in this work fell well below this threshold, exhibiting a low-resistance parallel-conduction path between the Ag and FTO electrodes that is inconsistent with a defect-free insulating ZnO layer. The wide spread of measured values (from fully shorted pads to ~ 107 kΩ) indicates that the magnitude of this parasitic conduction varies substantially from sample to sample, and in most cases from pad to pad on the same sample.

The observed spread of resistances does not admit a single uniform physical interpretation. Fully shorted devices ($R \ll 1\ \Omega$) are consistent with classical pinhole shorts: Ag-filled through-thickness holes in the ZnO that provide direct metallic contact between the electrodes and produce sub-ohm resistance set by the geometry of the local metal-metal contact. Finite-resistance samples (hundreds of ohms to tens of kilohms) cannot be explained by pinhole geometry because it would be unphysical. Finite-resistance conduction in the non-shorted samples is therefore most plausibly dominated by distributed bulk leakage through the ZnO film itself, arising from oxygen-vacancy donor electrons throughout the film volume, rather than by localized pinhole defects. This bulk-leakage interpretation is directly supported by the annealing-resistance correlation described previously (and more in depth below), since annealing modifies ZnO stoichiometry and oxygen-vacancy density throughout the film but does not affect the geometry of any existing pinhole defects.

Among devices that were not fully shorted, DC resistance correlated with annealing status: annealed samples read systematically higher resistance than as-deposited samples. Annealed sample 21 read approximately 107 kΩ, while unannealed sample 27 read approximately 12.5 kΩ. This matches the mechanism that oxygen vacancies in as-deposited ZnO act as n-type donors that lower bulk resistivity, while annealing in air at 500 °C refills a fraction of these vacancies via oxygen diffusion and raises it. Annealing, therefore, reduces the bulk-leakage component of parallel conduction.

C. Single-Event Transient Response

Sample 21, exhibiting the highest measured resistance of 107 kΩ, was selected for detailed electrical characterization as the device most likely to yield a detectable piezoelectric signal. When the instrumented device was subjected to isolated, discrete mechanical events (a single firm tap with the plastic probe tip, or a single press-and-hold-and-release cycle) no transient voltage response could be resolved above the system noise floor. This was true for taps of varying force, from gentle touches to deliberately firm knock-like impacts. This null single-event result is consistent with the expected piezoelectric response for a device with a 107 kΩ parallel shunt, since generated charge drains through the shunt nearly as fast as it is produced during a hand-delivered tap, limiting the peak terminal voltage to approximately the product of the instantaneous piezoelectric current and the shunt resistance.

Two factors determine the absolute amplitude of this single-event voltage, and both carry considerable uncertainty for the present devices and measurement conditions. The effective piezoelectric coefficient of PLD-grown thin-film ZnO varies over nearly an order of magnitude across the literature, depending sensitively on c-axis texture and deposition quality, and the specifics of hand-delivered mechanical excitation (peak force and rise time) similarly span a wide range across individual taps. Combined with the measured shunt resistance, these factors place the expected single-event voltage amplitude broadly in the range of tens to hundreds of microvolts referred to the sensor input (overlapping the 200–500 μV peak-to-peak noise floor of the measurement environment). Under these conditions, individual tap events produce transients of amplitude comparable to typical noise fluctuations and cannot be reliably distinguished from them by visual inspection of the Serial Plotter. The absence of a consistently visible single-tap response is therefore not evidence against piezoelectric activity in the film but rather a predicted consequence of single-event signal amplitudes falling near the instantaneous detection threshold set by ambient noise.

D. Cyclical Tapping and Coherent Signal Detection

When mechanical excitation was applied as a sustained rhythmic sequence (repeated firm taps on the Ag pad of Sample 21 at a rate of approximately 2 Hz, maintained continuously for several seconds) a clearly correlated cyclical variation appeared in the amplified voltage trace observed on the Arduino Serial Plotter. The temporal period of this variation matched the period of the applied mechanical stimulation; when the tapping rate was deliberately changed, the period of the voltage trace changed in a corresponding manner. Intermittent tapping with pauses produced an intermittent signal on the trace, with quiet intervals between trains, demonstrating tight temporal correlation between mechanical input and electrical output.

The amplitude of this correlated signal was of the same order as expected for a single tap on this device. Each tap produces a positive-polarity pulse on compression and a negative-polarity pulse on release; rhythmic tapping generates a train of alternating pulses whose peak-to-peak amplitude in a cycle is comparable to that of an individual tap. What made the signal detectable under rhythmic excitation, when individual taps were not, is not a change in per-event amplitude but rather a change in the observer's ability to extract a small signal from a larger noise background.

During a single discrete tap, both the signal and the ambient broadband noise occupy the same millisecond-scale window, and because the signal amplitude is comparable to or smaller than the noise, we could not reliably distinguish any single tap event from an ordinary noise fluctuation on the Serial Plotter. Under rhythmic tapping, in contrast, a clear periodic variation appeared on the voltage trace whose period tracked our applied tap rate: when we changed the tempo, the trace period changed; when we paused, the periodicity disappeared.

This pattern became recognizable even though individual taps did not, because rhythmic stimulation concentrates the signal at one specific frequency (the tap rate and its harmonics), while the dominant ambient noise is either broadband or concentrated at unrelated frequencies such as 60 Hz mains pickup. Over an observation interval containing many tap cycles, the periodic structure of this kind is distinguishable against broadband noise even when no single cycle exceeds the instantaneous noise amplitude (the same principle that underlies hardware lock-in amplification).

The observable correlation between our applied taps and the observed voltage oscillations is direct evidence that the signal originated as a response to our mechanical input rather than as noise or pickup. A genuine piezoelectric response must track the applied stress; the film develops a charge proportional to the instantaneous force, so a sequence of press-and-release cycles at a particular rate necessarily produces a corresponding sequence of alternating voltage pulses at that same rate. The correspondence we observed (appearance of periodicity precisely when we began tapping, its disappearance when we stopped, and its change of period when we changed tempo) is consistent with piezoelectric generation within the device.

E. Dependence of Signal Detectability on Sample Resistance

Sample 21 was the only device on which a correlated cyclical signal was observed, despite the application of identical mechanical stimulation to several other samples across the fabricated set. This selectivity reflects the overall crystallinity of the ZnO film, which simultaneously controls both prerequisites for a detectable piezoelectric response: a well-crystallized film has both a higher bulk resistance (fewer oxygen-vacancy donor electrons, hence larger shunt resistance and a larger terminal voltage) and a stronger preferential c-axis orientation (more fully aligned along the polar axis). These two properties are not independent; they both improve together with film crystal quality, which is in turn driven by the annealing process. Sample 21 was annealed and exhibited the strongest (002) c-axis growth in our XRD analysis, and was also the sample with the highest non-shorted DC resistance; both signatures are consistent with it being the most fully crystallized film that we have fabricated. No detectable piezoelectric signal was observed on any other sample, whether pinhole-shorted, non-annealed, or annealed with weaker c-axis texture, consistent with reduced film crystallinity in each of these cases.

F. Confirmation via Control Experiments

To discriminate a genuine piezoelectric origin of the observed cyclical signal on Sample 21 from candidate artifacts, the three control experiments described in the methods (tape-insulation control, electrode-polarity reversal control and off-device mechanical control) were executed in sequence. All three controls were performed on the same device and electrode pair and with identical amplifier settings immediately after the positive observation, to ensure that any changes in the signal were attributable to the experimental manipulation rather than to drift in the measurement conditions. It passed all three control tests.

The simultaneous satisfaction of all three tests, together with the force-correlated appearance and disappearance of the signal (which excludes purely environmental pickup unrelated to the stimulus), constitutes strong evidence that the observed cyclical voltage response on Sample 21 originates in genuine piezoelectric charge separation within the ZnO layer of the device.

V. DISCUSSION AND CONCLUSIONS

The results of this work show that ZnO thin films grown by pulsed laser deposition can be incorporated into a working thin-film device structure and can develop the crystallographic features needed for piezoelectric sensing. XRD measurements showed that annealing had a strong effect on film quality. In particular, Sample 21 exhibited a dominant ZnO (002) peak, reduced intensity of non-(00l) reflections, and narrower peak widths than the unannealed control, indicating stronger c-axis preferred orientation and larger crystallite size. Since the strongest piezoelectric response in ZnO is expected along the c-axis, these structural results show that the fabrication process was capable of producing films with the correct orientation for pressure sensing.

However, the electrical results show that achieving the correct crystal structure was not by itself enough to produce a strong and easily measurable device response. The DC resistance measurements revealed that all fabricated devices contained significant parasitic conduction between the Ag top electrode and the FTO bottom electrode. Some devices were completely shorted, while others showed finite but still relatively low resistance values. Even the best-performing sample, Sample 21, had a measured resistance of only about 107 kΩ, which is far below the megohm-scale resistance expected for an ideal insulating piezoelectric capacitor. This means that the fabricated devices behaved as leaky capacitors, with charge generated in the ZnO film able to drain away through a parallel shunt path before building a large terminal voltage. In practice, this leakage strongly limited the measurable electrical response.

The resistance data also provide an important interpretation of the role of annealing. Among samples that were not fully shorted, annealed devices consistently showed higher resistance than unannealed devices. For example, Sample 21 measured approximately 107 kΩ, while unannealed Sample 27 measured approximately 12.5 kΩ. This trend is consistent with the idea that annealing reduces oxygen-vacancy-related conduction in the ZnO film. In this project, annealing therefore improved the devices in two ways at once: it strengthened c-axis texture, which should increase piezoelectric charge generation, and it increased bulk resistance, which helps preserve that charge long enough to be detected electrically. This combined improvement is likely the main reason that Sample 21 was the only device to show a clearly correlated electrical response under mechanical stimulation.

The transient electrical measurements show the consequences of this leakage. Under isolated single-tap or single press-and-release events, Sample 21 produced no voltage transient that could be resolved above the 200–500 μV noise floor of the measurement system. This null result does not necessarily indicate absence of piezoelectric behavior. Rather, it is consistent with the expected behavior of a device that has both a small intrinsic signal and a finite shunt resistance. In such a device, the generated charge leaks away on a short timescale, reducing the peak terminal voltage. The estimated signal range for a single event overlaps the ambient laboratory noise level, so a genuine signal may still be present even if it cannot be distinguished from noise in an individual trace.

The most important electrical result of the project is that Sample 21 did show a clear response under rhythmic cyclical tapping. When the sample was tapped repeatedly at approximately 2 Hz, a correlated periodic voltage pattern appeared in the amplified output. When the tapping rate changed, the period of the observed voltage trace changed as well, and when tapping stopped, the periodic structure disappeared. This is significant because it shows that the device output tracked the applied mechanical stimulation in time. The fact that this signal became visible under repeated tapping but not under single taps is also physically reasonable. Rhythmic excitation does not necessarily increase the amplitude of each individual event, but it makes a weak signal easier to distinguish from broadband noise by concentrating it at a repeatable frequency. In this sense, the cyclical measurement acted like a simple coherence test: the signal became detectable because it repeated in a structured way, while the noise did not.

This interpretation is strengthened by the control experiments. The correlated cyclical signal persisted when an insulating tape layer was placed between the probe tip and the Ag electrode, which argues against triboelectric contact charging as the source. The signal also inverted cleanly when electrode polarity was reversed, which is the expected behavior for a real piezoelectric voltage but not for many common noise sources. Finally, no correlated signal was observed when mechanical stimulation was applied to the bare substrate away from the active electrode region, ruling out simple vibration coupling through the sample holder or substrate. Taken together, these controls provide strong evidence that the cyclical voltage response observed in Sample 21 originated from genuine piezoelectric charge separation in the ZnO layer.

An important conclusion from the full set of results is that the electrical response depended on both film crystallinity and film resistivity, and that these two factors improved together in the best annealed sample. Sample 21 was not only the most strongly c-axis-oriented film in the XRD analysis, but also the device with the highest measured non-shorted resistance and the only one that showed a correlated cyclical voltage response. This suggests that the successful operation of this device geometry requires both a film that can generate piezoelectric charge efficiently and a film that is electrically resistive enough to prevent that charge from being lost immediately to leakage. In other words, structural quality alone is not sufficient; electrical isolation is equally important.

Future work should therefore focus on improving the electrical quality of the device as much as the crystallographic quality of the ZnO film. Reducing pinhole shorts, increasing ZnO resistivity, and further refining the annealing process will likely improve charge retention and increase measurable voltage output. On the measurement side, a lower-noise setup with better shielding, more sensitive amplification, and a calibrated force-application method would make it possible to more directly compare measured response with the theoretical pressure-voltage model developed earlier in the paper. These changes would also help determine whether the observed cyclical response can be converted into a quantitatively reliable pressure measurement.

In conclusion, this project successfully fabricated ZnO/FTO/Ag thin-film devices, demonstrated that post-deposition annealing strongly improves ZnO c-axis texture and reduces leakage, and identified Sample 21 as the strongest candidate piezoelectric sensor produced in this work. Although no single-event voltage response could be resolved above the ambient noise floor, a mechanically correlated cyclical electrical response was observed in Sample 21 and passed multiple artifact-rejection control tests. The overall results therefore support the conclusion that piezoelectric response was present in the best device, while also showing that parasitic conduction and limited measurement sensitivity remain the main barriers to reliable quantitative sensing. This work establishes a strong proof of concept for ZnO thin-film pressure sensors in this geometry and clarifies the device and measurement improvements needed for future development.

VI. ACKNOWLEDGMENTS

We wish to thank Shane Brogan, David Stilwell, and Dr. Rene Lopez for their assistance and mentorship throughout the process. Additionally, we would like to thank Dr. Josh Chen for operating the XRD machinery.

[1] V. K. Samoei and A. H. Jayatissa, arXiv preprint arXiv:2110.13643 (2021).

[2] J. H. Choi, H. Tabata, and T. Kawai, Journal of Crystal Growth 10.1016/S0022-0248(01)01388-4 (2002).

[3] Özgür, Y. I. Alivov, C. Liu, A. Teke, M. A. Reshchikov, S. Doğan, V. Avrutin, S.-J. Cho, and H. Morkoç, Journal of Applied Physics **98**, 041301 (2005).